ACADEMIC PRESS

Available online at www.sciencedirect.com

SCIENCE DIRECT®

Journal of Computational Physics 184 (2003) 406–421

JOURNAL OF COMPUTATIONAL PHYSICS

www.elsevier.com/locate/jcp

Lattice Boltzmann method for moving boundaries

Pierre Lallemand [a], Li-Shi Luo [b,*]

[a] *Laboratoire CNRS-ASCI, Bâtiment 506, Université Paris-Sud (Paris XI Orsay), 91405 Orsay Cedex, France*
[b] *ICASE, MS 132C, NASA Langley Research Center, 3 West Reid Street, Building 1152, Hampton, VA 23681-2199, USA*

Received 27 July 2001; received in revised form 14 June 2002; accepted 30 September 2002

Abstract

We propose a lattice Boltzmann method to treat moving boundary problems for solid objects moving in a fluid. The method is based on the simple bounce-back boundary scheme and interpolations. The proposed method is tested in two flows past an impulsively started cylinder moving in a channel in two dimensions: (a) the flow past an impulsively started cylinder moving in a transient Couette flow; and (b) the flow past an impulsively started cylinder moving in a channel flow at rest. We obtain satisfactory results and also verify the Galilean invariance of the lattice Boltzmann method.

Keywords: Generalized lattice Boltzmann equation; Moving boundary; Galilean invariance; Flows past an impulsively started cylinder moving in a channel

1. Introduction

The lattice Boltzmann equation (LBE) is an explicit time marching finite difference scheme of the continuous Boltzmann equation in phase space and time [1–3]. The LBE method has a underlying Cartesian lattice grid in space as a consequence of the symmetry of the discrete velocity set and the fact that the lattice spacing δ_x is related to time step size δ_t by $\delta_x = c\delta_t$, where c is the basic unit of the discrete velocity set. This makes the LBE method a very simple scheme consisting of two essential steps: collision and advection. The collision models various interactions among fluid particles and the advection simply moves particles from one grid point to the other according to their velocities. The simplicity and kinetic nature of the LBE method are among its appealing features.

One area in the LBE method which attracts much attention is the boundary conditions in the LBE method. In particular, a much studied and often used boundary condition is the bounce-back boundary condition which mimics the particle–boundary interaction for no-slip boundary condition by reversing the momentum of the particle colliding with an impenetrable and rigid wall. The bounce-back boundary

* Corresponding author. Tel.: +757-864-8006; fax: +757-864-6134.
E-mail addresses: lalleman@asci.fr (P. Lallemand), luo@icase.edu (L.-S. Luo).

0021-9991/02/$ - see front matter
PII: S0021-9991(02)00022-0

condition is most easy to implement and thus most often used in the LBE simulations. It is well understood now that the bounce-back boundary condition is indeed second-order accurate when the actual boundary position is considered to be off the grid point where the bounce-back collision takes place [4–8]. The bounce-back boundary condition is accurate and thus appropriate for very simple boundary geometries made of straight lines. In dealing with complex geometry of arbitrary curvatures, there are two strategies in the LBE method. One strategy is to use the body-fitted mesh and employs interpolations throughout the entire mesh [9,10] in addition to the advection process because the computational mesh does not overlap with the underlying Cartesian lattice [11,12], bounce-back boundary conditions are applied to the boundary nodes. The other strategy is to maintain the regular Cartesian mesh and apply interpolations to track the position of the boundary and the bounce-back boundary conditions are executed at the boundary locations which may be off the grid cartesian points [13,14]. These methods are mostly applied to simulations of stationary objects in fluids. We shall follow the latter approach in the present study.

The lattice Boltzmann method has also been successfully applied to simulations of particulate suspensions in fluids [15–17]. In the LBE simulations of the particulate suspensions in a flow, the curved boundaries of the particles are usually approximated by zig-zag staircase thus bounce-back boundary condition can be directly applied. Despite the success of the LBE method in this area, there is no rigorous theory on the treatment of moving boundaries. In this work, we present our first attempt to systematically study the boundary boundary problem within the framework of the LBE. The method studied in this work is an extension of the method based on bounce-back and interpolations for curved boundaries proposed by Bouzidi et al. [13].

This paper is organized as follows. Section 2 describes the generalized lattice Boltzmann equation (GLBE) of d'Humières [18–21]. Among its features, the GLBE has superior stability over the popular lattice BGK equation [22,23]. Section 3 discusses the boundary conditions for the moving boundary problem, preluded by a brief introduction of the method to treat curved boundaries proposed by Bouzidi et al. [13]. Section 4 presents the numerical results. We simulate a cylinder asymmetrically placed in a channel in two dimensions with two types of initial conditions. The first is an impulsively started cylinder with a constant velocity moving in a transient Couette flow. And the second is an impulsively started cylinder with a constant velocity in the channel flow at rest. We compare the results of moving boundary simulations with that of fixed boundary. We therefore verify the Galilean invariance of the LBE method. Finally, Section 5 discusses possible directions to improve the method for moving boundary proposed in this work and concludes the paper.

2. Description of the model

We consider a two-dimensional LBE model with nine discrete velocities (the D2Q9 model) on a square grid with grid spacing δ_x. In the advection step of the LBE, particles move from one node of the grid to one of its neighbors as illustrated in Fig. 1. The discrete velocities are given by

$$\boldsymbol{e}_\alpha = \begin{cases} (0,0), & \alpha = 0, \\ (\cos[(\alpha-1)\pi/2], \sin[(\alpha-1)\pi/2])c, & \alpha = 1\text{–}4, \\ (\cos[(2\alpha-9)\pi/4], \sin[(2\alpha-9)\pi/4])\sqrt{2}c, & \alpha = 5\text{–}8, \end{cases} \tag{1}$$

where $c = \delta_x/\delta_t$, and the duration of the time step δ_t is assumed to be unity. Therefore $c = 1$ in the units of $\delta_x = 1$ and $\delta_t = 1$. (In what follows all quantities are given in non-dimensional units, normalized by the grid spacing δ_x and time step δ_t.) At any (discrete) time t_n $(= n\delta_t)$, the LBE fluid is then characterized by the populations of the nine velocities at each node of the computational domain

$$|f(\boldsymbol{r}_j, t_n)\rangle \equiv (f_0(\boldsymbol{r}_j, t_n), f_1(\boldsymbol{r}_j, t_n), \ldots, f_8(\boldsymbol{r}_j, t_n))^{\mathsf{T}}, \tag{2}$$

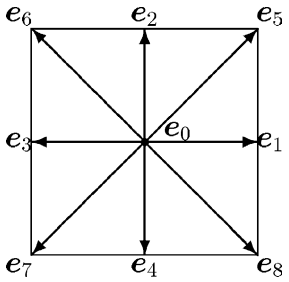

Fig. 1. Discrete velocities of the D2Q9 model on a two-dimensional square lattice.

where T is the transpose operator. Here upon the Dirac notations of bra, $\langle\cdot|$, and ket, $|\cdot\rangle$, vectors are used to denote row and column vectors, respectively. The time evolution of the state of the fluid follows the general equation

$$|f(\boldsymbol{r}_j + \boldsymbol{e}_\alpha\delta_t, t_n + \delta_t)\rangle = |f(\boldsymbol{r}_j, t_n)\rangle + \Omega|f(\boldsymbol{r}_j, t_n)\rangle, \tag{3}$$

where collisions are symbolically represented by the operator Ω.

The LBE is thus a trajectory in a $9 \times N$ phase space with discrete time, where N is the number of spatial grid points under consideration. At each grid point, the state of the system can be represented by a vector $|f\rangle$ defined by Eq. (2) in a nine-dimensional space $\mathbb{F}$. We can make a linear transformation from $\mathbb{F}$ space to some other space that may be more convenient. In particular, we shall use physically meaningful moments of the quantities f_α that span space $\mathbb{M}$. As proposed by d'Humières [18], we shall use the GLBE in which the collision process is executed in moment space $\mathbb{M}$.

The mapping between moment space $\mathbb{M}$ and discrete velocity space $\mathbb{F}$ is one-to-one and defined by the linear transformation M which maps a vector $|f\rangle$ in $\mathbb{F}$ to a vector $|\hat{f}\rangle$ in $\mathbb{M}$, i.e.,

$$|\hat{f}\rangle = \mathsf{M}|f\rangle \quad \text{and} \quad |f\rangle = \mathsf{M}^{-1}|\hat{f}\rangle. \tag{4}$$

The spatial part of the evolution in Eq. (3) is easiest to handle in space $\mathbb{F}$, whereas the collision part in Eq. (3) is preferably treated in space $\mathbb{M}$ both for physical and computational reasons.

With reference to kinetic theory of gases [24,25] and making use of the symmetries of the discrete velocity set, M is constructed as the following:

$$\mathsf{M} = \begin{pmatrix} \langle m_1| \\ \langle m_2| \\ \langle m_3| \\ \langle m_4| \\ \langle m_5| \\ \langle m_6| \\ \langle m_7| \\ \langle m_8| \\ \langle m_9| \end{pmatrix} = \begin{pmatrix} 1 & 1 & 1 & 1 & 1 & 1 & 1 & 1 & 1 \\ -4 & -1 & -1 & -1 & -1 & 2 & 2 & 2 & 2 \\ 4 & -2 & -2 & -2 & -2 & 1 & 1 & 1 & 1 \\ 0 & 1 & 0 & -1 & 0 & 1 & -1 & -1 & 1 \\ 0 & -2 & 0 & 2 & 0 & 1 & -1 & -1 & 1 \\ 0 & 0 & 1 & 0 & -1 & 1 & 1 & -1 & -1 \\ 0 & 0 & -2 & 0 & 2 & 1 & 1 & -1 & -1 \\ 0 & 1 & -1 & 1 & -1 & 0 & 0 & 0 & 0 \\ 0 & 0 & 0 & 0 & 0 & 1 & -1 & 1 & -1 \end{pmatrix}$$
$$= (|m_1\rangle, |m_2\rangle, |m_3\rangle, |m_4\rangle, |m_5\rangle, |m_6\rangle, |m_7\rangle, |m_8\rangle, |m_9\rangle)^{\mathsf{T}}. \tag{5}$$

The components of the row vector $\langle m_\beta|$ in matrix M are polynomials of the x and y components of the velocities $\{\boldsymbol{e}_\alpha\}$, $e_{\alpha,x}$, and $e_{\alpha,y}$. The vectors $\langle m_\beta|$, $\beta = 1, 2, \ldots, 9$, are orthogonalized by the Gram–Schmidt procedure. Specifically,

$$
\begin{aligned}
|m_1\rangle_\alpha &= \|\boldsymbol{e}_\alpha\|^0 = 1,\\
|m_2\rangle_\alpha &= -4\|\boldsymbol{e}_\alpha\|^0 + 3(e_{\alpha,x}^2 + e_{\alpha,y}^2),\\
|m_3\rangle_\alpha &= 4\|\boldsymbol{e}_\alpha\|^0 - \frac{21}{2}(e_{\alpha,x}^2 + e_{\alpha,y}^2) + \frac{9}{2}(e_{\alpha,x}^2 + e_{\alpha,y}^2)^2,\\
|m_4\rangle_\alpha &= e_{\alpha,x},\\
|m_5\rangle_\alpha &= [-5\|\boldsymbol{e}_\alpha\|^0 + 3(e_{\alpha,x}^2 + e_{\alpha,y}^2)]e_{\alpha,x},\\
|m_6\rangle_\alpha &= e_{\alpha,y},\\
|m_7\rangle_\alpha &= [-5\|\boldsymbol{e}_\alpha\|^0 + 3(e_{\alpha,x}^2 + e_{\alpha,y}^2)]e_{\alpha,y},\\
|m_8\rangle_\alpha &= e_{\alpha,x}^2 - e_{\alpha,y}^2,\\
|m_9\rangle_\alpha &= e_{\alpha,x}e_{\alpha,y}.
\end{aligned}
\tag{6}
$$

Note that vectors $|m_\beta\rangle$ (and their duals $\langle m_\beta|$) are not normalized in order to simplify the expression of M (in integers). It is interesting to point out that the moments $m_\alpha = \langle m_\alpha|f\rangle$ are the restriction to a finite number of velocities of the low order moments of the continuous velocity distribution function used in kinetic theory. We may give a physical interpretation to the quantities defined above and define the local state in $\mathbb{M}$ space as

$$
|\hat{f}\rangle = (\rho, e, \varepsilon, j_x, q_x, j_y, q_y, p_{xx}, p_{xy})^{\mathsf{T}}, \tag{7}
$$

where $m_1 = \rho$ is the density, $m_2 = e$ is related to the kinetic energy, $m_3 = \varepsilon$ is related to the kinetic energy square. $m_4 = j_x$ and $m_6 = j_y$ are x and y components of the momentum density, $m_5 = q_x$ and $m_7 = q_y$ are proportional to the x and y components of the energy flux, and $m_8 = p_{xx}$ and $m_9 = p_{xy}$ are proportional to the diagonal and off-diagonal components of the viscous stress tensor.

The collision process in the LBE model is simply modeled by a relaxation process to the chosen equilibria with multiple relaxation times. Based upon kinetic theory, we use the following equilibrium distribution functions for the non-conserved moments, which depend only on the conserved moments, i.e., ρ, and $\boldsymbol{j} = (j_x, j_y)$:

$$
e^{(\mathrm{eq})} = -2\rho + \frac{3}{\rho}(j_x^2 + j_y^2), \tag{8a}
$$

$$
\varepsilon^{(\mathrm{eq})} = \rho - \frac{3}{\rho}(j_x^2 + j_y^2), \tag{8b}
$$

$$
q_x^{(\mathrm{eq})} = -j_x, \tag{8c}
$$

$$
q_y^{(\mathrm{eq})} = -j_y, \tag{8d}
$$

$$
p_{xx}^{(\mathrm{eq})} = \frac{1}{\rho}\left(j_x^2 - j_y^2\right), \tag{8e}
$$

$$
p_{xy}^{(\mathrm{eq})} = \frac{1}{\rho}j_x j_y. \tag{8f}
$$

It should be noted that the energy is not considered as a conserved quantity here because the model is athermal. (The model does not possess sufficient degrees of freedom to accommodate the dynamics of

locally stable heat transport.) With the above equilibrium functions, the sound speed of the system is $c_s = 1/\sqrt{3}$.

In what follows the idea of the "incompressible" LBE [26] is applied to the above equilibria so that ρ is replaced by a constant ρ_0 $(= 1)$ in the denominators of Eqs. (8a), (8e), and (8f). This choice allows for better comparison with other incompressible simulations and simpler algebra while retaining correct acoustics. This approximation means that we neglect terms of order $O(M^2)$, where M is the Mach number. A simple improvement to include compressibility is to consider fluctuation of ρ with the following approximation:

$$\frac{1}{\rho} \approx \frac{1}{\rho_0}(2\rho_0 - \rho), \tag{9}$$

where $\rho = \rho_0 + \delta\rho$.

The collision process is modeled by the following relaxation equations:

$$|\hat{f}^*\rangle = |\hat{f}\rangle - \mathsf{S}[|\hat{f}\rangle - |\hat{f}^{(\mathrm{eq})}\rangle], \tag{10}$$

where $|\hat{f}^*\rangle$ denotes the post-collision state, and S is the diagonal relaxation matrix

$$\mathsf{S} = \mathrm{diag}(0, s_2, s_3, 0, s_5, 0, s_7, s_8, s_9). \tag{11}$$

The model reduces to the usual lattice BGK model if all the relaxation parameters are set to be a single relaxation time τ, i.e., $s_\alpha = 1/\tau$. It should be stressed that the relaxation parameters are not independent in some cases, as shown in [19,27]. The constraints of isotropy may lead to some relationships between these relaxation parameters [19,27]. Obviously, the usual lattice BGK model cannot satisfy such constraints.

The LBE model described above is in essence a spectral-type algorithm. The distribution functions are represented in the orthogonal basis functions constructed from monomials $e_{\alpha,x}^n e_{\alpha,x}^m$ (n and $m = 1, 2, \ldots$) [18,19,27]. The orthogonal basis functions span moment space $\mathbb{M}$. Collision is performed in the space $\mathbb{M}$ among the moments. Then moments are mapped back to the physical space $\mathbb{V}$ of $|f\rangle$ to perform advection. The additional computational effort due to the linear transformations between space $\mathbb{V}$ and $\mathbb{M}$ is rather insignificant (ca. 10%), provided some care is given in programming. It is worth the effort in programming compared to the simple BGK scheme as it is quite superior in terms of numerical stability, can be made much less sensitive to spurious acoustic waves and is necessary for isotropy for some models, like the efficient 13-velocity model [20].

3. Boundary condition for moving boundary

Our treatment for a moving boundary is a simple extension of the treatment for a curved boundary proposed by Bouzidi et al. [13]. This treatment for a curved boundary is a combination of the bounce-back scheme and interpolations. For the sake of simplicity, this boundary condition is illustrated in Fig. 2 for an idealized situation in two dimensions. Consider a wall located at an arbitrary position $\boldsymbol{r}_w$ between two grid sites $\boldsymbol{r}_j$ and $\boldsymbol{r}_s$, and $\boldsymbol{r}_s$ is situated inside the non-fluid region – the shaded area depicted in Fig. 2. The parameter q defines the fraction in fluid region of a grid spacing intersected by the boundary, i.e., $q \equiv |\boldsymbol{r}_j - \boldsymbol{r}_w|/\delta_x$. It is well understood that the bounce-back boundary conditions place the wall about one-half grid spacing beyond the last fluid node [5], i.e., $q = 1/2$, as shown in Fig. 2(a). That is, even though the bounce-back boundary is executed on the node $\boldsymbol{r}_j$, the actual position of the wall is located at $\boldsymbol{r}_w$ which is about one-half grid spacing beyond the last fluid node $\boldsymbol{r}_j$. Thus one could intuitively picture the bounce-back boundary as the following: the particle with the velocity $\boldsymbol{e}_1$, starting from $\boldsymbol{r}_j$, travels from left to right, hits the wall at $\boldsymbol{r}_w$, reverses its momentum, then returns to its starting point $\boldsymbol{r}_j$. This imaginary particle

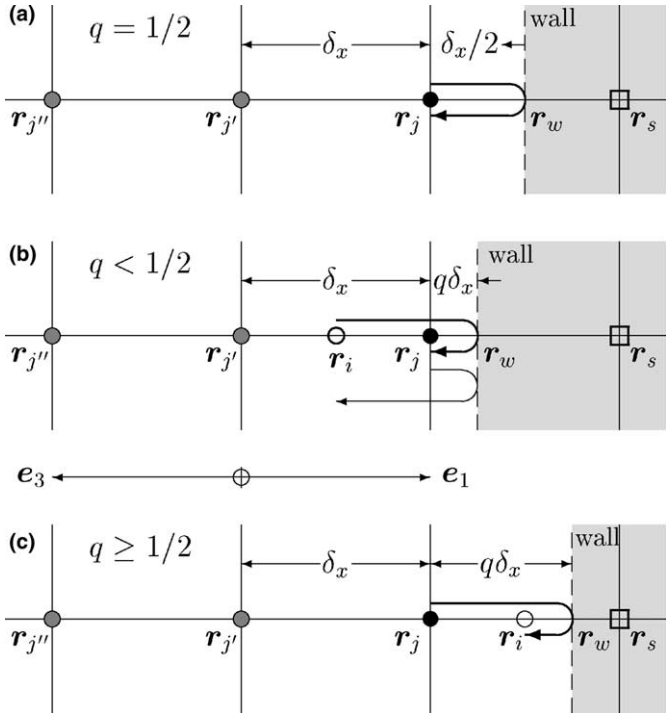

Fig. 2. Illustration of the boundary conditions for a rigid wall located arbitrarily between two grid sites in one dimension. The thin solid lines are the grid lines, the dashed line is the boundary location situated arbitrarily between two grids. Shaded disks are the fluid nodes, and the disks (●) are the fluid nodes next to boundary. Circles (○) are located in the fluid region but not on grid nodes. The square boxes (□) are within the non-fluid region. The thick arrows represent the trajectory of a particle interacting with the wall, described in Eqs. (14a) and (14b). The distribution functions at the locations indicated by disks are used to interpolate the distribution function at the location marked by the circles (○). (a) $q \equiv |\boldsymbol{r}_j - \boldsymbol{r}_w|/\delta_x = 1/2$. This is the perfect bounce-back condition – no interpolations needed. (b) $q < 1/2$. (c) $q \geqslant 1/2$.

trajectory is indicated by the thick bent arrow in Fig. 2(a). The total distance traveled by the particle is one grid spacing δ_x during the bounce-back collision, according to Fig. 2(a). Therefore, one can imagine that the bounce-back collision either takes one time step or no time at all, corresponding to two implementations of the bounce-back scheme: link and node implementations [15,16], respectively. The difference between these two implementations is that the bounced-back distributions (e.g., f_3 in Fig. 2(a)) at the boundary nodes in the link implementation is one time step behind that in the node implementation. This difference vanishes for the steady-state calculations, although these two implementations of the bounce-back boundary conditions have different stability characteristics, because the link implementation destroys the parity symmetry on a boundary node, whereas the node implementation preserves the parity symmetry. However, one cannot determine a priori the advantage of one implementation over the other, because the features of the two implementations also strongly depend on the precise location of the boundary and the local flow structure. This issue certainly deserves further study. It is also important to stress the fact that the actual boundary location is not affected by the two different implementations of the bounce-back scheme – it is always about one-half grid spacing beyond the last fluid node [5].

With the picture for the simple bounce-back scheme in mind, let us first consider the situation depicted in Fig. 2(b) in detail for the case of $q < 1/2$. At time t the distribution function of the particle with velocity pointing to the wall ($\boldsymbol{e}_1$ in Fig. 2) at the grid point $\boldsymbol{r}_j$ (a fluid node) would end up at the point $\boldsymbol{r}_i$ located at a

distance $(1-2q)\delta_x$ away from the grid point $\boldsymbol{r}_j$, after the bounce-back collision, as indicated by the thin bent arrow in Fig. 2(b). Because $\boldsymbol{r}_i$ is not a grid point, the value of f_3 at the grid point $\boldsymbol{r}_j$ needs to be reconstructed. Noticing that f_1 starting from point $\boldsymbol{r}_i$ would become f_3 at the grid point $\boldsymbol{r}_j$ after the bounce-back collision with the wall, we construct the values of f_1 at the point $\boldsymbol{r}_i$ by a quadratic interpolation involving values of f_1 at the three locations: $f_1(\boldsymbol{r}_j), f_1(\boldsymbol{r}_{j'}) = f_1(\boldsymbol{r}_j - \boldsymbol{e}_1\delta_t)$ and $f_1(\boldsymbol{r}_{j''}) = f_1(\boldsymbol{r}_j - 2\boldsymbol{e}_1\delta_t)$. In a similar manner, for the case of $q \geqslant 1/2$ depicted in Fig. 2(c), we can construct $f_3(\boldsymbol{r}_j)$ by a quadratic interpolation involving $f_3(\boldsymbol{r}_i)$ that is equal to $f_1(\boldsymbol{r}_j)$ before the bounce-back collision, and the values of f_3 at the nodes after collision and advection, i.e., $f_3(\boldsymbol{r}_{j'})$, and $f_3(\boldsymbol{r}_{j''})$. Therefore the interpolations are applied differently for the two cases:

- For $q < 1/2$, interpolate before propagation and bounce-back collision.
- For $q \geqslant 1/2$, interpolate after propagation and bounce-back collision.

We do so to avoid the use of extrapolations in the boundary conditions for the sake of numerical stability. This leads to the following interpolation formulas (where the notations $\hat{f}_\alpha$ and f_α denote the post-collision distribution functions before and after advection):

$$f_{\bar{\alpha}}(\boldsymbol{r}_j,t) = q(1+2q)\hat{f}_\alpha(\boldsymbol{r}_j,t) + (1-4q^2)\hat{f}_\alpha(\boldsymbol{r}_{j'},t) - q(1-2q)\hat{f}_\alpha(\boldsymbol{r}_{j''},t) + 3w_\alpha(\boldsymbol{e}_\alpha\cdot\boldsymbol{u}_w), \quad q<\frac{1}{2}, \tag{12a}$$

$$f_{\bar{\alpha}}(\boldsymbol{r}_j,t) = \frac{1}{q(2q+1)}\hat{f}_\alpha(\boldsymbol{r}_j,t) + \frac{(2q-1)}{q}f_{\bar{\alpha}}(\boldsymbol{r}_{j'},t) - \frac{(2q-1)}{(2q+1)}f_{\bar{\alpha}}(\boldsymbol{r}_{j''},t) + \frac{3w_\alpha}{q(2q+1)}(\boldsymbol{e}_\alpha\cdot\boldsymbol{u}_w), \quad q\geqslant\frac{1}{2}, \tag{12b}$$

$$w_\alpha = \begin{cases} 2/9, & \alpha = 1\text{–}4, \\ 2/36, & \alpha = 5\text{–}8, \end{cases} \tag{13}$$

where $f_{\bar{\alpha}}$ is the distribution function of the velocity $\boldsymbol{e}_{\bar{\alpha}} \equiv -\boldsymbol{e}_\alpha$, and $\boldsymbol{u}_w$ is the velocity of the moving wall at the point $\boldsymbol{r}_w$ in Fig. 2. The case $\alpha = 0$ is not considered as f_0 is known at grid point $\boldsymbol{r}_j$ after collision and is not affected by the advection step. The term in proportion to $w_\alpha(\boldsymbol{e}_\alpha\cdot\boldsymbol{u}_w)$ is the momentum exerted on the fluid by the moving wall of velocity $\boldsymbol{u}_w$. It can be derived as the following. Suppose a forcing term F_α is introduced due to the fluid–wall interaction, the mass conservation $\sum_\alpha F_\alpha = 0$ and the momentum conservation $\sum_\alpha \boldsymbol{e}_\alpha F_\alpha = \rho_0\boldsymbol{u}_w$ immediately lead to $F_\alpha = 3w_\alpha(\boldsymbol{e}_\alpha\cdot\boldsymbol{u}_w)$ [28,29]. The correction $1/[q(2q+1)]$ for the case of $q \geqslant 1/2$ is obtained by considering the analytic solution for the Couette flow.

In practice, it is more efficient to combine collision and advection into one step. Because advection simply corresponds to shifts of indices labeling spatial nodes of $\{f_\alpha\}$, the actual formulas used in simulations are

$$f_{\bar{\alpha}}(\boldsymbol{r}_j,t) = q(1+2q)f_\alpha(\boldsymbol{r}_j+\boldsymbol{e}_\alpha\delta_t,t) + (1-4q^2)f_\alpha(\boldsymbol{r}_j,t) - q(1-2q)f_\alpha(\boldsymbol{r}_j-\boldsymbol{e}_\alpha\delta_t,t) + 3w_\alpha(\boldsymbol{e}_\alpha\cdot\boldsymbol{u}_w), \quad q<\frac{1}{2}, \tag{14a}$$

$$f_{\bar{\alpha}}(\boldsymbol{r}_j,t) = \frac{1}{q(2q+1)}f_\alpha(\boldsymbol{r}_j+\boldsymbol{e}_\alpha\delta_t,t) + \frac{(2q-1)}{q}f_{\bar{\alpha}}(\boldsymbol{r}_j-\boldsymbol{e}_\alpha\delta_t,t) - \frac{(2q-1)}{(2q+1)}f_{\bar{\alpha}}(\boldsymbol{r}_j-2\boldsymbol{e}_\alpha\delta_t,t) + \frac{3w_\alpha}{q(2q+1)}(\boldsymbol{e}_\alpha\cdot\boldsymbol{u}_w), \quad q\geqslant\frac{1}{2}. \tag{14b}$$

The above formulas are implemented as follows. The collision–advection process including the bounce-back collision with boundaries are divided in the following five steps:

- *Step* 1: Compute moments at all fluid nodes.
- *Step* 2: Relax the non-conserved moments at all fluid nodes, add momentum change if an external force is presented.
- *Step* 3: Compute the post-collision distributions $\{f_\alpha\}$ at all fluid nodes.
- *Step* 4: Advect $\{f_\alpha\}$ throughout the system, including all fluid and non-fluid nodes. Some distributions will be advected from fluid nodes to non-fluid nodes, and some from non-fluid nodes to fluid nodes.
- *Step 5*: Recompute the distributions that are advected from non-fluid nodes to fluid nodes according to Eq. (14a) or (14b), depending on the precise location of the boundary (i.e., the value of q).

When boundaries lie in between two nodes of two grid points, the above implementation is equivalent to the "node implementation" of the bounce-back scheme, i.e., the bounce-back collision does not take time.

Note that Eq. (14a) is an upwind interpolation, while Eq. (14b) is a downwind interpolation. Both equations reduce to the elementary bounce-back scheme when $q = 1/2$. The above formulas have combined advection and collision steps together, in addition to a correction of about one half grid spacing due to the bounce-back collision, as illustrated in Fig. 2(a). These formulas are compatible with a quadratic spatial variation of the fluid velocity $\boldsymbol{u}$ in the vicinity of the boundary and a linear dependence of the equilibrium distribution functions on the flow velocity $\boldsymbol{u}$.

The interpolations introduced in the above formulas obviously compromise the mass conservation. However, this shortcoming can be overcome by considering a more elaborate construction of the local equilibrium distribution [30], which leads the exact solution for quadratic flows such as the Poiseuille flow [30]. It should be emphasized that Eqs. (14a) and (14b) only involve the position of a boundary relative to the computational mesh of Cartesian grids, therefore they can be readily applied in three dimensions. Some three-dimensional LBE simulations have been carried out this way [14,20,21].

Because the bounce-back scheme is completely independent of the collision process, one can use the simple BGK algorithm as one wishes. This would only alter Steps 1–3 as discussed above. The treatment for boundaries remains the same regardless whatever collision algorithm is used.

To extend the above boundary conditions for a moving boundary illustrated in Fig. 3, provided that the velocity of the moving wall, $\boldsymbol{u}_w$, is not too fast compared to the sound speed c_s in the system, one must also solve the following problem. When a grid point moves out of the non-fluid region into the fluid region to

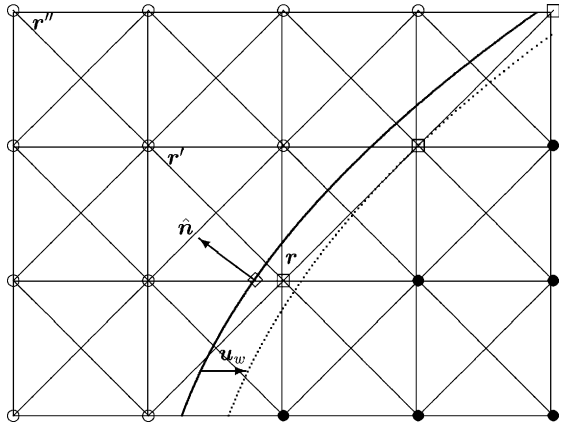

Fig. 3. Illustration of a moving boundary with velocity $\boldsymbol{u}_w$. The circles (○) and disks (●) denote the fluid and non-fluid nodes, respectively. The squares (□) denote the nodes becoming fluid nodes from the non-fluid nodes at one time step δ_t (= 1). The solid and dotted curves are the wall boundary at time t and $t + \delta_t$, respectively.

become a fluid node (indicated by □ in Fig. 3, one must specify some number of unknown distribution functions on this node. We use a second order extrapolation to compute the unknown distribution functions along the direction of a chosen discrete velocity $\boldsymbol{e}_\alpha$ which maximizes the quantity $\hat{\boldsymbol{n}} \cdot \boldsymbol{e}_\alpha$, where $\hat{\boldsymbol{n}}$ is the out-normal vector of the wall at the point (marked by ◇ in Fig. 3 through which the node moves to fluid region. For example, the unknown distribution functions $\{f_\alpha(\boldsymbol{r})\}$ at node $\boldsymbol{r}$ as depicted in Fig. 3 can be given by the following extrapolation formula:

$$f_\alpha(\boldsymbol{r}) = 3f_\alpha(\boldsymbol{r}') - 3f_\alpha(\boldsymbol{r}'') + f_\alpha(\boldsymbol{r}'' + \boldsymbol{e}_6).$$

Obviously the method to compute values of the unknown distribution functions (on the nodes which move from non-fluid to fluid region) is not unique. One could, for instance, compute the equilibrium distribution functions at $\boldsymbol{r}$ by using the velocity $\boldsymbol{u}_w$ of the moving boundary and the averaged density in the system ρ_0 or otherwise obtained locally averaged density, and use the equilibrium distribution functions for the unknown distribution functions. Alternatively, one could also systematically update the distribution functions in the non-fluid regions by performing collisions as in the fluid regions while velocity is kept at the moving velocity $\boldsymbol{u}_w$ of the solid object. All these schemes produce similar results.

As depicted in Fig. 2, the momentum transfer occurred near the boundary along the direction of $\boldsymbol{e}_\alpha$ is equal to

$$\delta \boldsymbol{p}_\alpha = \boldsymbol{e}_\alpha [f_\alpha(\boldsymbol{r}_w, t) + f_{\bar{\alpha}}(\boldsymbol{r}_j, t)]. \tag{15}$$

The above formula gives the momentum flux through any boundary normal to $\boldsymbol{e}_\alpha$ located between point $\boldsymbol{r}_w$ and point $\boldsymbol{r}_j$ in Fig. 2. In the simulations, we use the above formula to evaluate momentum exchange in the interaction between fluid and solid bodies.

4. Simulations

We conduct numerical simulations to investigate the accuracy of the proposed boundary conditions for a moving boundary. We use a cylinder asymmetrically placed in a channel in two dimensions as the basic configuration, as shown in Fig. 4. With different boundary conditions and initial conditions, we can simulate different flow situations in the channel. The flow simulations can be performed in two frames of reference. First, the position of the cylinder is fixed on the computational mesh, such that the boundary of the cylinder is also at rest; and second, the cylinder is moving at a constant velocity with respect to the mesh thus the boundary of the cylinder is moving. However, the relative motion between the cylinder and the flow in the channel remains the same in either cases by matching the boundary conditions and forcing in two frames of reference. By directly comparing the results obtained from these two different settings, one

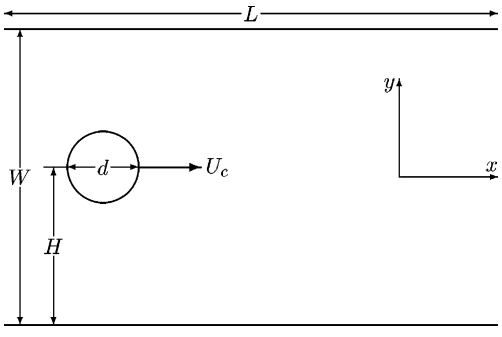

Fig. 4. Configuration of a two-dimensional flow past a cylinder asymmetrically placed in a channel.

can test not only the accuracy of the proposed moving boundary conditions, but also the Galilean invariance of the LBE method.

The geometric configuration of the following flow simulations is depicted in Fig. 4. A cylinder of diameter d is asymmetrically placed in a channel of width W and length L. The distance between the cylinder center and the lower wall of the channel is H. The flow is moving from left to right in the channel.

We use the following values for three relaxation parameters in the generalized LBE scheme: $s_2 = s_5 = 1.5$ and $s_3 = 1.4$, unless otherwise stated (cf. [19] for the significance and proper choice of these relaxation parameters).

4.1. A cylinder in a transient two-dimensional Couette flow

We first simulate a transient Couette flow past the cylinder moving with a constant velocity $(U_c, 0)$ in x-direction in the channel. Initially the flow is a rest. At time $t = 0$, the upper and lower walls of the channel impulsively start to slide in x-direction with velocity $(U_0, 0)$ or $(-U_0, 0)$, respectively. Without the cylinder, the flow in the channel evolves to the steady Couette flow. The cylinder is moving in the fluid with a constant speed U_c in x-direction. For the sake of simplicity, the periodic boundary conditions are used in x-direction.

A typical computational domain of the channel is $L \times W = 201 \times 101$. The diameter of the cylinder is $d/W = 0.25$ ($d = 25.25$). The magnitude of moving velocity at channel walls is $U_0 = 0.1$. The viscosity of the flow is $\nu = c_s^2(1/s_8 - 1/2) \approx 1/9$ ($s_8 = 1.2$). The shear rate of the flow is defined as $\kappa = 2U_0/W$. The Reynolds number is

$$Re = \frac{\kappa d^2}{\nu}. \tag{16}$$

With the parameters given above, the Reynolds number is approximately 11.36.

The center of the cylinder is initially located at $(x_0, y_0) = (30, 54)$, which is off the centerline of the channel. We define the eccentricity (in y-direction) of cylinder with respect the channel centerline as

$$\varepsilon = \frac{2H}{W} - 1, \tag{17}$$

where H is the y coordinate of the cylinder center. For the above configuration, $\varepsilon = 1/15$. The cylinder is moving with a constant speed $U_c = 0.02$ in x-direction.

In the frame of reference at rest, the cylinder is moving with the speed U_c with respect to the mesh, thus the boundary of the cylinder is moving with respect to the mesh. However, in the frame of reference moving with a constant velocity U_c, the boundary of the cylinder is fixed with respect to the mesh. In this moving frame of reference, the velocities of the upper and lower walls of the channel are $(U_0 - U_c)$ and $-(U_0 + U_c)$, respectively. We simulate the flow in both frames of reference.

Fig. 5 shows the measurements of total force $\boldsymbol{F} = (F_x, F_y)$ and torque Γ on the cylinder as functions of time obtained using two frames of reference, either at rest or moving with the cylinder center. We use the second-order extrapolations to compute the unknown distribution functions on the nodes emerging from within the cylinder into the fluid region. The x and y component of the force, F_x and F_y, are the drag and lift forces, respectively. The forces obtained with the moving boundary (in the rest frame of reference) show a very small fluctuation around the results computed with fixed boundary (in the moving frame of reference). The magnitude of fluctuation is remarkably small considering the radius of the cylinder r is only 12.625 grid spacing.

Fig. 6 shows the same results as in Fig. 5, except that the unknown distribution functions on the nodes emerging from within the cylinder into the fluid region are approximated by the equilibrium distribution

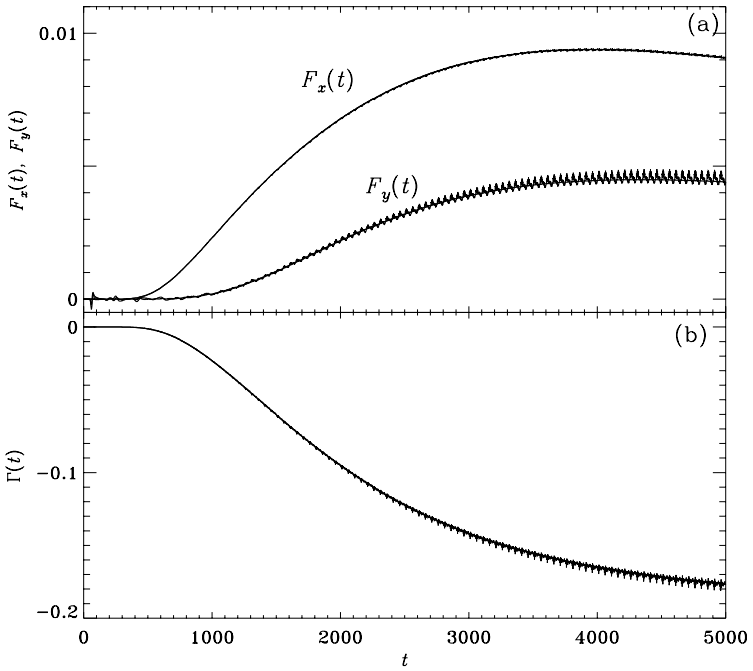

Fig. 5. A cylinder moving with a constant speed $U_c = 0.02$ along x-direction in a transient two-dimensional Couette flow at $Re = 11.36$. Total force (F_x, F_y) and torque Γ on the cylinder measured as functions of time t. The second-order extrapolation scheme was used to compute the unknown distribution functions on the nodes coming out from the non-fluid region to the fluid region. (a) The drag force $f_x(t)$ and lift force $f_y(t)$; and (b) total torque $\Gamma(t)$.

functions with the velocity of the cylinder and the averaged density in the system. The fluctuations in the drag and lift forces and the torque are significantly larger than the results obtained by using the second-order extrapolations for the unknown distribution functions.

In both cases (by using either the second-order extrapolations or the equilibrium distribution functions for the unknown distribution functions), the averaged total force and torque obtained in the simulations with moving boundary are very close to the results obtained in simulations with fixed boundary. The fluctuation has a period of $1/U_c \approx 50$. Higher frequency fluctuations are due to the movements of grid points in and out the region inside the cylinder. The results clearly demonstrate the fact that the LBE method is indeed Galilean invariant.

Fig. 7 shows the contour lines of the stream function at $t = 5000$. We compare the results obtained by fixed cylinder boundary (in the frame of reference moving with the cylinder) and by moving cylinder boundary (in the frame of reference at rest). The second-order extrapolation is used to compute the unknown distribution functions on the nodes coming out from the non-fluid region to the fluid region. The difference between the two results is very little. We also compute the L^2-normed difference between the two velocity fields

$$\Delta_2(t) = \sqrt{\frac{\sum_i \|\boldsymbol{u}_1(\boldsymbol{r}_i, t) - \boldsymbol{u}_0(\boldsymbol{r}_i, t)\|^2}{\sum_i \|\boldsymbol{u}_0(\boldsymbol{r}_i, t)\|^2}}, \tag{18}$$

where $\boldsymbol{u}_1$ and $\boldsymbol{u}_0$ are the velocity fields computed with moving boundary and fixed boundary, respectively. At $t = 5000$, we found that $\Delta_2 \approx 0.12\%$.

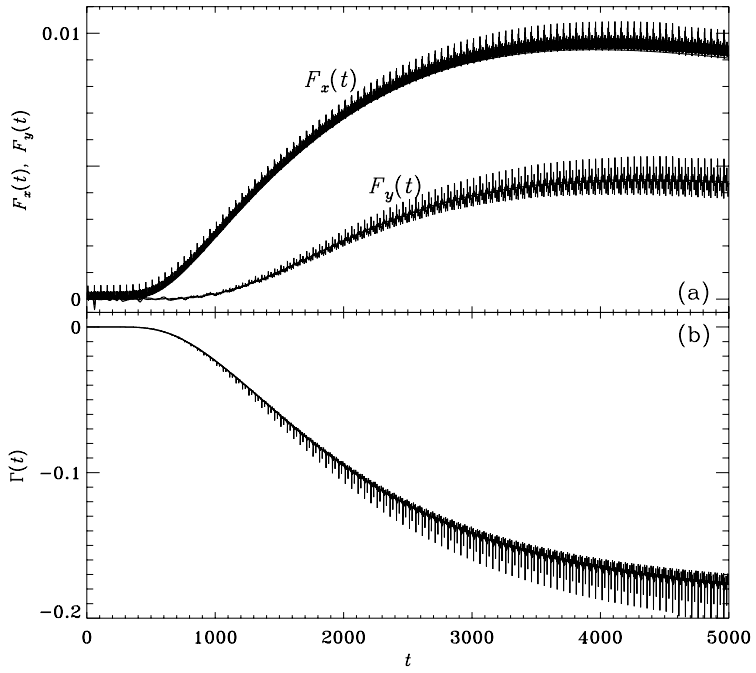

Fig. 6. Same as Fig. 5. The equilibrium distribution functions are used for the unknown distribution functions. (a) The drag force $f_x(t)$ and lift force $f_y(t)$; (b) total torque $\Gamma(t)$. Note the fluctuations are much larger than the results shown in Fig. 5.

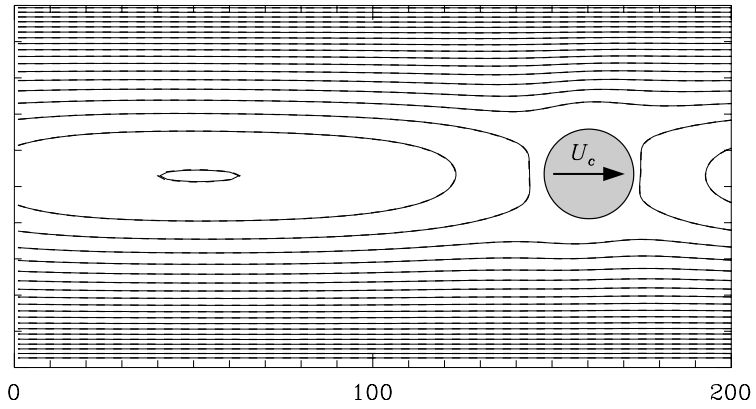

Fig. 7. A cylinder moving with a constant speed $U_c = 0.02$ along x-direction in a transient two-dimensional Couette flow at $Re = 11.36$. Contour lines of the stream function at $t = 5000$. The solid lines and dashed lines are the results obtained by fixed cylinder boundary (in the frame of reference moving with the cylinder) and by moving cylinder boundary (in the frame of reference at rest).

4.2. Flow past a impulsively started cylinder in a channel

Our second simulation is the flow of a impulsively started cylinder in a channel. The flow configuration is similar to that of the previous case. At time $t = 0$, the fluid in the channel is at rest and the cylinder is impulsively started to move with a constant speed $U_c = 0.04$ in x-direction. This is equivalent to the

following initial conditions of the flow: the fluid is given an uniform speed $U_f = -0.04 = -U_c$, so are the lower and upper walls given a constant speed $U_w = -0.04 = -U_c$, and the cylinder is at rest. Periodic boundary conditions are applied in x-direction for both cases. The former case is in the frame of reference at rest, thus the boundary of the cylinder is moving with respect to the mesh. The latter is in the frame of reference moving with the cylinder, thus the boundary of the cylinder is fixed while the fluid is moving with opposite velocity. In both cases, the channel has dimensions $L \times W = 1001 \times 101$, the radius $r = 12$, $H = 54$, and the initial position of the cylinder is $(x_0, y_0) = (60.3, 54)$. The viscosity v is such that the Reynolds number $Re = 2rU_c/v = 200$.

Fig. 8 shows the drag and lift experienced by the cylinder as functions of time. Shown in the figure are three sets of results. First, the flow was computed with the fixed boundary of the cylinder. The computations with boundary of cylinder moving with respect to the mesh were performed by using either the second-order extrapolations or the equilibrium distribution functions for the unknown distribution functions on the nodes emerging from within the cylinder next to the boundary. Fig. 8(a) and 8(b) compare the results of moving boundary calculations by using the second-order extrapolations and the equilibrium distribution functions with the results by using fixed boundary, respectively. The fluctuations due the movement of the boundary are comparable in either cases. However, there is a phase difference between the results obtained by using moving or fixed boundary. This phase shift is due to the higher order non-Galilean effects in the sound speed and viscosities [19].

We compare in Fig. 9 the stream function for the two computations corresponding to Fig. 8(a) at $t = 15{,}000$. The phase shift due to the higher order non-Galilean effects is apparent.

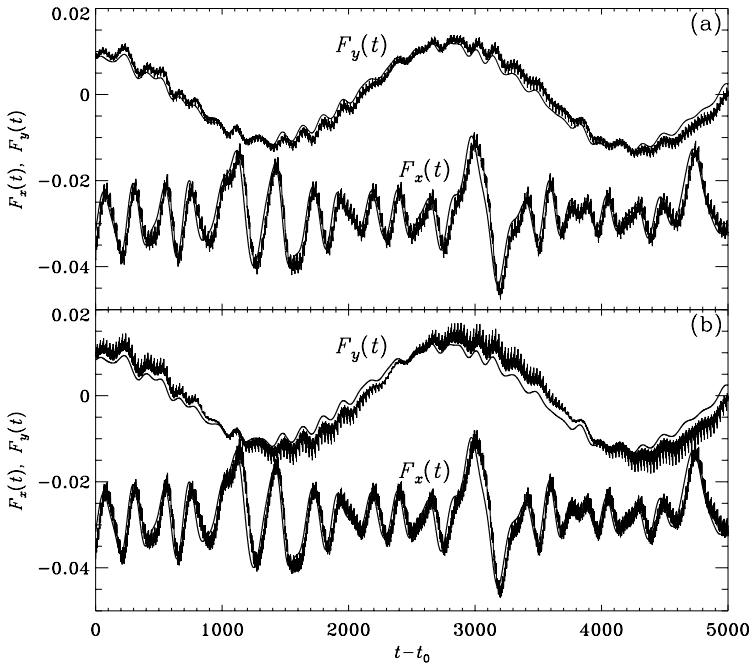

Fig. 8. An impulsively started cylinder moving with a constant speed $U_c = 0.04$ in x-direction in a two-dimensional channel with periodic boundary condition in x-direction. Reynolds number $Re = 200$. Total force (F_x, F_y) on the cylinder measured as functions of time t after an initial run time $t_0 = 14{,}000$. The smooth lines are the results obtained in the frame of reference moving with the cylinder (the fixed boundary calculation) and the fluctuating lines are the results obtained in the frame of reference at rest (the moving boundary calculations). (a) The second-order extrapolations are used to compute the unknown distribution functions, and (b) the equilibrium distribution functions are used for the unknown distribution functions.

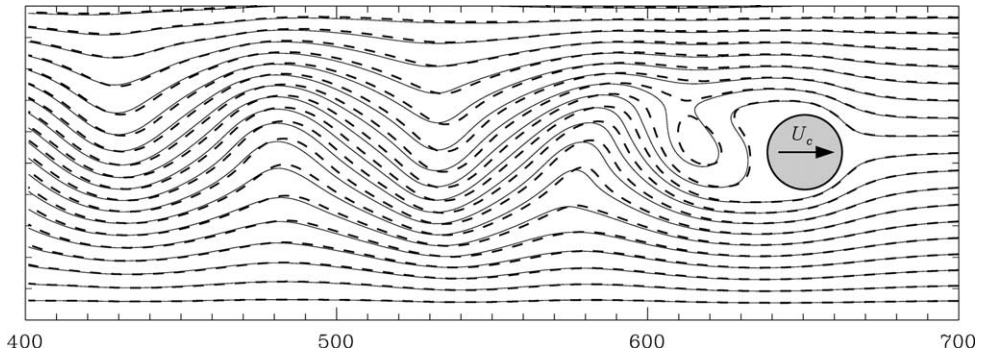

Fig. 9. The stream functions of the flow at $t = 15{,}000$ correspond to the two calculations in Fig. 8(a). Solid lines and dashed lines correspond to results with fixed and moving boundary of the cylinder, respectively.

5. Conclusion and discussion

In this work we have proposed a lattice Boltzmann scheme to handle moving boundary problems. The proposed scheme is robust, stable, and easy to implement. The proposed scheme is tested in the simulations of two-dimensional flows past an impulsively started cylinder asymmetrically placed in a channel with different initial conditions. The results obtained with either moving boundary or fixed boundary agree well with each other. The simulations also verify the Galilean invariance of the lattice Boltzmann method. The proposed scheme can also be applied in three dimensions.

We note that the treatment of the moving boundary considered here is independent of the collision model in the LBE method. Therefore, it can be applied to any lattice Boltzmann methods with either multiple-relaxation-time (MRT) or single-relaxation-time (BGK) models. That is, the GLBE model is not critical as far as the boundary conditions are concerned. Nevertheless, the MRT models do render much better numerical stability [19,21], and this is a crucial issue especially when the Mach number is not negligibly small [19].

We observed in the simulations that, although the LBE method can be used to accurately compute the total drag and lift forces and total torque exerted on a object moving in a flow, the result of the force at a particular point at the boundary may not be as accurate as the integrated results. The reason is that there is a spatial fluctuation in the force depending on the location of the boundary relative to the mesh. There are several reasons that directly contribute to the fluctuation. First of all, there are grid points moving from non-fluid region to fluid region or vice versa. Thus the number of fluid nodes is not conserved. That means the volume (or area) occupied by a rigid moving body is not a constant. As soon as a grid node leaving the non-fluid region becomes a fluid node, it is immediately treated indiscriminately as other fluid nodes in the fluid region without taking into account, for instance, the cell associated with the node is only partially in the fluid region. It would certainly be more sensible to treat these nodes with a finite-volume methodology. However, this is yet to be formulated on a rigorous basis. Secondly, when a grid point just emerges from the non-fluid region into the fluid region, the distribution functions must be constructed on this point. The error in the construction can be an immediate contribution to the fluctuation. And finally, near a fluid node next to a boundary, the number of the lattice lines intersected with the boundary varies. This number also varies in time as the boundary is moving. This number directly affects the accuracy of the local fluid fields and its variation in both space and time therefore also contributes to the fluctuation. However, this local fluctuation seems canceled out in the integrated quantities, such as the drag and lift forces.

There are other sources of error observed in the simulations. First, the compressibility is one important source of error because of the velocity-dependence of the transport coefficient. That is a higher order effect

of non-Galilean invariance. Such effect can be reduced by increasing the number of discrete velocities. Secondly, the number of the grid points in the fluid region (or non-fluid region) is not a constant. The grid points moving in and out of the fluid region to and from the non-fluid region have an immediate effect on the momentum transfer at the boundary near their vicinities. This effect directly leads to a fluctuation in the force. And thirdly, the interpolations destroy the mass conservation near the boundary. The inaccuracy in the evaluation of the momentum transfer at boundary leads to a net mass flux. To reduce or eliminate the aforementioned errors are the interest of our research in the future.

Acknowledgements

P.L. would like to acknowledge the support from ICASE for his visit to ICASE in 2001, during which part of this work was performed. L.S.L. would like to acknowledge the partial support from CNRS for his visit to ASCI Laboratory in 2001 during which part of this work was performed, and partial support from NASA Langley Research Center under the program of Innovative Algorithms for Aerospace Engineering Analysis and Optimization and the United States Air Force Office for Scientific Research under Grant No. F49620-01-1-0142 (technical monitor Dr. J. Tishkoff). The authors would like to thank Prof. D. Qi for stimulating discussions, are grateful to Dr. M. Salas, the director of ICASE, for his support and encouragement of this work.

References

[1] X. He, L.-S. Luo, A priori derivation of the lattice Boltzmann equation, Phys. Rev. E 55 (1997) R6333–R6336.
[2] X. He, L.-S. Luo, Theory of the lattice Boltzmann method: from the Boltzmann equation to the lattice Boltzmann equation, Phys. Rev. E 56 (1997) 6811–6817.
[3] T. Abe, Derivation of the lattice Boltzmann method by means of the discrete ordinate method for the Boltzmann equation, J. Comput. Phys. 131 (1997) 241–246.
[4] I. Ginzbourg, P.M. Alder, Boundary flow condition analysis for the three-dimensional lattice Boltzmann model, J. Phys. II (France) 4 (1994) 191–214.
[5] I. Ginzbourg, D. d'Humières, Local second-order boundary method for lattice Boltzmann models, J. Statist. Phys. 84 (1996) 927–971.
[6] I. Ginzbourg, D. d'Humières, Local second-order boundary method for lattice Boltzmann models: Part II. Application to complex geometries, Preprint, 1996.
[7] L.-S. Luo, Analytic solutions of linearized lattice Boltzmann equation for simple flows, J. Statist. Phys. 88 (1997) 913–926.
[8] X. He, Q. Zou, L.-S. Luo, M. Dembo, Analytic solutions and analysis on non-slip boundary condition for the lattice Boltzmann BGK model, J. Statist. Phys. 87 (1997) 115–136.
[9] X. He, L.-S. Luo, M. Dembo, Some progress in lattice Boltzmann method: Part I. Nonuniform mesh grids, J. Comput. Phys. 129 (1996) 357–363.
[10] X. He, L.-S. Luo, M. Dembo, Some progress in lattice Boltzmann method: enhancement of Reynolds number in simulations, Physica A 239 (1997) 276–285.
[11] X. He, G.D. Doolen, Lattice Boltzmann method on a curvilinear coordinate system: vortex shedding behind a circular cylinder, Phys. Rev. E 56 (1997) 434–440.
[12] X. He, G.D. Doolen, Lattice Boltzmann method on curvilinear coordinates system: flow around a circular cylinder, J. Comput. Phys. 134 (1997) 306–315.
[13] M. Bouzidi, M. Firdaouss, P. Lallemand, Momentum transfer of a lattice-Boltzmann fluid with boundaries, Phys. Fluids 13 (2002) 3452–3459.
[14] D. Yu, R. Mei, W. Shyy, L.-S. Luo, Force evaluation in the lattice Boltzmann method involving curved geometry, Phys. Rev. E 65 (2002) 041203.
[15] A.J.C. Ladd, Numerical simulations of particulate suspensions via a discretized Boltzmann equation: Part 1. Theoretical foundation, J. Fluid Mech. 271 (1994) 285–309.
[16] A.J.C. Ladd, Numerical simulations of particulate suspensions via a discretized Boltzmann equation: Part 2. Numerical results, J. Fluid Mech. 271 (1994) 311–339.

[17] D. Qi, Lattice Boltzmann simulations of particles in non-zero-Reynolds-number flows, J. Fluid Mech. 385 (1999) 41–62.
[18] D. d'Humières, Generalized lattice-Boltzmann equations, in: B.D. Shizgal, D.P. Weaver (Eds.), Rarefied Gas Dynamics: Theory and Simulations, Progress in Astronautics and Aeronautics, vol. 159, AIAA, Washington, DC, 1992, pp. 450–458.
[19] P. Lallemand, L.-S. Luo, Theory of the lattice Boltzmann method: Dispersion, dissipation, isotropy, Galilean invariance, and stability, Phys. Rev. E 61 (2000) 6546–6562.
[20] D. d'Humières, M. Bouzidi, P. Lallemand, Thirteen-velocity three-dimensional lattice Boltzmann model, Phys. Rev. E 63 (2001) 066702.
[21] D. d'Humières, I. Ginzburg, M. Kraftzyck, P. Lallemand, L.-S. Luo, Multiple-relaxation-time lattice Boltzmann models in three-dimensions, Proc. Roy. Soc. London A 360 (2002) 437–451.
[22] Y.H. Qian, D. d'Humières, P. Lallemand, Lattice BGK models for Navier–Stokes equation, Europhys. Lett. 17 (1992) 479–484.
[23] H. Chen, S. Chen, W.H. Matthaeus, Recovery of the Navier–Stokes equations using a lattice-gas Boltzmann method, Phys. Rev. A 45 (1992) R5339–R5342.
[24] J.O. Hirschfelder, C.F. Curtiss, R.B. Bird, Molecular Theory of Gases and Liquids, Wiley, New York, 1954.
[25] S. Harris, An Introduction to the Theory of the Boltzmann Equation, Holt, Rinehart, and Winston, New York, 1971.
[26] X. He, L.-S. Luo, Lattice Boltzmann model for the incompressible Navier–Stokes equation, J. Statist. Phys. 88 (1997) 927–944.
[27] M. Bouzidi, D. d'Humières, P. Lallemand, L.-S. Luo, Lattice Boltzmann equation on a two-dimensional rectangular grid, J. Comput. Phys. 172 (2001) 704–717.
[28] L.-S. Luo, Unified theory of the lattice Boltzmann models for nonideal gases, Phys. Rev. Lett. 81 (1998) 1618–1621.
[29] L.-S. Luo, Theory of the lattice Boltzmann method: lattice Boltzmann models for nonideal gases, Phys. Rev. E 62 (2000) 4982–4996.
[30] I. Ginzburg, D. d'Humières, Multi-reflection boundary conditions for lattice Boltzmann models, ITWM Report (38)-2002 (available at http://www.itwm.uni-kl.de/).